Published in final edited form as:
Oral Oncol. 2013 October ; 49(10): 1025–1031. doi:10.1016/j.oraloncology.2013.07.009.

Study of Functional Infrared Imaging for Early Detection of Mucositis in Locally Advanced Head and Neck Cancer Treated With Chemoradiotherapy

Ezra E.W. Cohen[1,4,†], **Omar Ahmed**[1], **Masha Kocherginsky**[2], **Galyna Shustakova**[1,6], **Emily Kistner-Griffin**[2,x], **Joseph K. Salama**[3,*], **Volodymyr Yefremenko**[5], and **Valentyn Novosad**[5]

Valentyn Novosad: Novosad@anl.gov

[1]Department of Medicine, University of Chicago

[2]Department of Health Studies, University of Chicago

[3]Department of Radiation and Cellular Oncology, University of Chicago

[4]University of Chicago Comprehensive Cancer Center

[5]Material Science Division, Argonne National Laboratory

[6]B.Verkin Institute for Low Temperature Physics and Engineering, Kharkiv 61103, Ukraine

Abstract

Background and Purpose—Chemoradiotherapy (CRT) has led to improved efficacy in treating locally advanced squamous cell carcinoma of the head and neck (LA-SCCHN) but has led to almost universal in-field mucositis. Patients treated with the same regimen often have differences in mucositis occurrence and severity. Mucositis induced via radiation is known to represent an intense inflammatory response histologically. We hypothesized that patients destined to display severe mucocutaneous toxicity would demonstrate greater alterations in thermal intensity early in therapy than identically treated counterparts. This will allow identification of patients that will require more intensive supportive care using thermal imaging technology.

Materials and Methods—Subjects with LA-SCCHN (oral cavity or oropharynx) being treated with the identical chemoradiotherapy regimen underwent baseline and weekly thermal imaging. Changes in skin temperature caused by mucositis and dermatitis compared with a reference area (T were calculated and correlated to grade of mucositis based on NCI-CTCAE 3.0.

Results—Thirty-four subjects were enrolled. Grade 3 mucositis and dermatitis was observed in 53% and 21%, respectively. We observed a statistically significant positive association between an early rise in T and mucositis grade (p value=0.03).

Conclusions—Thermal imaging is able to detect small and early changes in skin surface temperature that may be associated with development of mucositis in patients being treated with chemoradiotherapy.

[†]Corresponding author: Ezra Cohen, 900 East 57th Street, Room 7146, Chicago, IL, 60637, ecohen@medicine.bsd.uchicago.edu, fax 773 702 9268.
[*]Currently: Department of Radiation Oncology, Duke University, Durham, NC
[x]Currently: Hollings Cancer Center at the Medical University of South Carolina

Indexing Key Words

Mucositis; Chemoradiation Therapy; Head and Neck Cancer; Imaging

Introduction

Approximately 40,000 new cases of head and neck cancer (HNC) are diagnosed annually in the United States[1]. Of these patients, two-thirds present with locoregionally advanced disease (American Joint Committee on Cancer [AJCC] stage III or IV). Concurrent CRT has led to improved locoregional control, disease-free and overall survival in randomized clinical trials, and allows for organ preservation[2]. Therefore, concurrent CRT has become a standard of care for the treatment of locally advanced HNC[3]. Recent studies have reported 60-70% long-term survivorship with curative intent when using aggressive regimens[4,5]. Although CRT is associated with improved efficacy, it is accompanied by an increase in toxicity, in particular mucositis, which is now almost universal[6]. Mucositis, and its clinical sequelae, are consistently reported as the most bothersome side effects of CRT in HNC patients and often require narcotic analgesia[7]. In addition, mucositis can lead to nutritional deficits requiring enteral feeding, dehydration, and treatment compromise. Therefore, mucositis presents a difficult challenge in the management of locally advanced HNC patients.

There is a large variability in mucositis severity between patients; some of which is accounted for by radiotherapy dosing, fractionation, and treatment volume. However, mucositis severity differs between patients treated with the same treatment regimen[8]. Unfortunately, by the time an individual develops severe mucositis, therapy is well underway and the only recourse is to interrupt treatment or provide aggressive supportive care. The former has detrimental effects on disease control and the latter often involves invasive procedures such as instillation of a feeding tube.

There are genetic syndromes that predispose patients to adverse events from radiotherapy including Fanconi anemia or ataxia-telangiectasia. Many of these syndromes involve DNA repair mechanisms and have spurred research into functional assays to predict radiosensitivity in individuals who do not harbor known genetic defects, with the assumption that there is a genetic basis for the observed phenotype[9,10]. Conversely, cytokine release after tissue injury has been well documented and specific markers have been associated with radiotherapy[11,12]. These assays, although promising, are not yet in widespread use and still need to be fully validated. Currently, there is no applicable test for clinical use in predicting which individuals will eventually develop dose limiting or severe mucositis during CRT.

Functional thermal imaging has been used in clinical medicine for over four decades and has been advocated as a tool in breast cancer detection and prognostication, burn injury assessment, vascular disease states, and as an aid in the medical battlefield[13,14]. Infrared imaging is a non-invasive technique that allows the examiner to visualize and quantify changes in skin or mucosal surface temperature[13]. In fact, recent evidence supports that ΔT, the difference between mean values of skin area temperature of the affected area and the unaffected reference area, is a valid measure of burn severity that can be used to guide early surgical interventions[15].

We developed a system where infrared light naturally emitted from the skin surface is collected with a mirror-based scanning device and then focused with optical lenses on a high-sensitivity detector. The generated electrical signal is amplified and converted into digital data flow that is visualized in color on a monitor. This visual image graphically maps

the spatial distribution of body temperature. The spectrum of colors indicates an increase or decrease in the amount of infrared radiation being emitted from the body surface. Given a high degree of thermal symmetry in the normal body, subtle abnormal temperature asymmetry can be identified.

As a remote and non-invasive technique, the infrared imaging is absolutely safe for patients and is similar to imaging procedures with photo cameras sensitive to infrared light. The device[16] used in this study, developed at Argonne National Laboratory (ANL), is universal with a re-programmable microprocessor for testing various detector units and equipped with a laptop computer. The hardware is located in a small box, and consists of infrared optics, small cryostat, low-noise preamplifier, analog-to-digital converter, and microprocessor electronic module.

Radiotherapy associated mucositis manifests initially as erythematous areas in the treatment field. These phenotypic changes are accompanied by an intense inflammatory response, histologically. There is scant data regarding the temperature of these reactions, but it is likely that, as with other inflammatory lesions, there would be a measurable thermal difference between treated areas before and after commencing radiotherapy. We hypothesized that patients destined to display severe mucocutaneous toxicity would demonstrate greater alterations in thermal intensity early in therapy than identically treated counterparts. G-tube dependence during treatment is one of the dreaded sequelae of severe mucocutaneous toxicity. Currently, there is no universal rule for the timing of g-tube insertion, while some institutions insert them prophylactically prior to RT for all patients, others insert them only when oral intake is compromised. Therefore, detection of these early changes with the imaging modality described would be immensely valuable in identifying only a subset of patients who would require early feeding tube insertion for nutritional needs. This also could be valuable for identification of patients requiring more intensive supportive care, institution of preventative agents, or those who may be candidates for de-intensification of therapy to avoid serious toxicity.

Methods

Patient Selection and Chemoradiotherapy Treatment

Eligible subjects were required to have primary tumors of the oral cavity or oropharynx to allow visualization of the area of interest within the radiated field. Patients with active inflammatory or infectious oral lesions were excluded. All subjects were required to be treated with concurrent chemoradiotherapy on an FHX-based regimen involving twice daily radiation (1.5 Gy per fraction). Chemoradiotherapy was administered on a week-on/week-off basis that lasted 9 weeks and allowed imaging and assessment prior to the start of each treatment week. Subjects were followed for toxicity for a total of 14 weeks from the start of treatment. The University of Chicago Institutional Review Board approved the study and all subjects were required to provide informed consent prior to participation.

Thermal and mucositis measurement

As previously described [17] a thermal imaging system was utilized for temperature mapping. In order to ensure measurements were carried out under conditions to prevent exogenous temperature change, the specific conditions were used: control for distance between subject and camera (~1m); room temperature (23-24°C); absence of direct solar or electric lighting and heaters; adaptation time (subjects were asked to remain in sitting position for approximately 5 minutes prior to imaging); patients were restricted from drinking hot or cold water 10 to 15 minutes prior to measurement; and room area (~15 m^2). NCI-CTCAE 3.0 was used to grade mucositis.

A relative temperature scale was employed for quantitative analysis of the thermal images. In this case the accuracy of measurements was limited by the temperature sensitivity of the system ±0.06°C [17]. The skin temperature near the medial angle of one eye was defined as the reference to create a relative temperature scale for every patient. This area was not subjected to irradiation. Each patient was imaged prior to starting chemoradiotherapy (baseline session 1) and before each subsequent cycle of therapy at cumulative radiotherapy doses of 15, 30, 45, and 60 Gy (i.e. just prior to start of Cycles 2-4). Ten frontal, lateral and semi-profile thermal images were obtained at each session.

Thermal imaging data processing and quantitative estimation

For the thermal image analysis we only considered the areas below the imaginary line between the ear lobes and tip of the nose, eliminating from consideration lips, open mouth area, and single pustules. In addition, the area between nostrils and upper lip was eliminated because its temperature depends on respiratory rate. The lower imaging limit was approximately the clavicles and sternal notch.

Reference temperature T_{ref} for every session was defined on the frontal image as the average temperature over the eyes' medial angle spots (red spots on Fig.1). If the temperature difference between the left and right eye spots was more than 0.1 °C, we chose only the spot with lower temperature to define T_{ref}. Since the size and location of hyperthermal areas both in absolute and relative temperature scales (with $T \geq T_{ref}$) varied from session to session (Fig.2), consistently defining the "area of interest" across sessions was an important methodological task for our analyses. Three different approaches were considered to define of the "area of interest" in parallel:

Approach 1—Within the analyzed area of every thermal image from each session we identified the point with highest temperature, T_{max}, and marked an area of hyperthermia with the temperature $T \geq 0.98\ T_{max}$ around this point. This area was defined as the "area of interest for Approach 1".

Approach 2—Here we considered Session 2 (after the delivery of 15 Gy in Cycle 1 and just prior to the start of Cycle 2) as the reference session to define the "area of interest for Approach 2". On each image from this session, we circled an "area of interest for Approach 2" ($\approx$30 cm^2) approximately surrounding the "area of interest for Approach 1". We tracked the regions with the same shape, size, and location on the corresponding images from all other sessions (Figure 3). This approach allows for a defined area of interest that does not change size and location from session to session.

Approach 3—This approach incorporated radiotherapy planning volumes. After analyzing coronal, transverse, and sagittal orientations of radiation treatment planning volumes, we selected the most suitable thermal image of the surface closest to the irradiated area. On the thermal image, we mapped the point on the face or neck skin surface with the minimal distance from the "irradiation point of interest" (center of tumor) on the radiation planning images. The "area of interest for Approach 3" was then marked around this point, with the shape approximately equal to the projection of "irradiation space of interest" (tumor) on the skin surface (Figure 4). The area of interest changed from session to session.

For each "area of interest" in each session *i* we the calculated average temperature $(T_{ave})_i$, and the differences from the reference $T_{ref,i}$ temperature: $\Delta T_i = T_i - T_{ref,i}$.

Quality of Life Assessments

The Performance Status Scale for Head and Neck Cancer (PSS-HN) including the three subscales of normalcy of diet, eating in public, and understandability of speech and the McMaster Radiotherapy Questionnaire which quantifies patients' perception of the frequency and severity of radiation-related side effects were administered at every imaging session.

Statistical Considerations

Three thermal images (frontal, lateral and semi-profile) were obtained during each of five sessions. The difference between average temperature within the "area of interest" relative to the reference temperature, $\Delta T_i = T_i - T_{ref,i}$, was calculated for each image based on two definitions of the "area of interest" (Approaches 1 and 2). Average of T_i's across the 3 images, Ave(T_i), was also calculated for each session. Correlation (P, rho) between Ave(T_i) for the two approaches was calculated for each session. A repeated measures analysis of variance model was also used, with ΔT_i for Approach 1 as the response variable and ΔT_i for Approach 2 as the predictor, adjusting for treatment cycle. Within-subject correlation between serial measurements throughout treatment was modeled using AR(1) covariance structure.

Early changes in temperature, ($\Delta T_1 - \Delta T_0$) and (Ave(ΔT_1) - Ave(ΔT_0)), were defined based on the changes from baseline to end of Cycle 1. Average toxicity grade was determined for the subsequent duration of treatment (Cycles 2-5). For mucositis and dermatitis, linear regression models were used to examine the relationship between early temperature changes and subsequent toxicity. The effect of early temperature changes on weight loss (continuous outcome) was also assessed using linear regression. Logistic regression models were used for G-tube placement (yes/no).

Results

Thirty-four subjects were enrolled between July 2008 and August 2009 (Table 1). One subject withdrew consent and one did not have baseline imaging; neither is included in the analysis. The median dose of radiotherapy administered was 74 Gy.

In-field radiation mucositis and dermatitis were assessed on a weekly basis (Figure 5). Grade 3 mucositis rates were highest by 5 weeks where it was observed in 18 patients (53%). Grade 3 dermatitis was most prevalent at 9 weeks where it was observed in 7 patients (21%). One patient developed grade 4 dermatitis at week 7. All subjects developed at least grade 2 mucositis during treatment.

Thermal intensity increased in the area of interest in all subjects progressively through treatment. There was high correlation between the average of the 3-image (frontal and two lateral) ΔT_{ave} obtained with Approaches 1 and 2, with correlation coefficients ranging from 0.664 to 0.905 (Supp. Figure 1). Repeated measures using the analysis of variance model of the relationship between two approaches, adjusted for treatment cycle, also demonstrated that the two approaches were strongly correlated ($p < 0.0001$).

To investigate the utility of thermal imaging as an early marker for subsequent toxicity, early changes in ΔT from baseline to end of Cycle 1, ($\Delta T_1 - \Delta T_0$), were correlated with the average and highest grade mucositis during subsequent treatment. For Approach 1, no statistically significant association between early changes in ΔT and average mucositis grade were found in separate linear regression models for each image type (Supp. Figure 2). However, using Approach 2, the association between early changes in ΔT was statistically significant ($p=0.03$) for frontal images. Based on this model, for a 1°C increase in (ΔT_1 -

ΔT_0) the average mucositis grade during Cycles 2- 5 of treatment increases by 0.157 (Figure 6A).

When an early change in ΔT averaged over the three images was considered (Ave(ΔT_1) - Ave(ΔT_0)), the effect was close to being statistically significant for Approach 2 (p=0.06). For each 1°C increase in (Ave(ΔT_1) - Ave(ΔT_0)), the average mucositis grade during treatment increased by 0.178 (Figure 6B). We also analyzed the same parameters using approach 3 but did not find statistical significance.

The relationship between T and dermatitis, weight loss, and gastrostomy tube requirement were also analyzed. No significant relationship was observed between early changes in temperature averaged across the three images (Ave(ΔT_1) - Ave(ΔT_0)) and subsequent dermatitis (p=0.48 and p=0.69 for Approaches 1 and 2, respectively), weight loss (p=0.23 and p=0.22 for Approaches 1 and 2, respectively), or feeding tube placement (p=0.42 and p=0.9022 for Approaches 1 and 2, respectively), although patients who required G-tube had a slightly greater increase in (Ave(ΔT_1) - Ave(ΔT_0)) than those who did not (0.878 vs. 0.724).

Discussion

Prediction of mucositis severity in individual patients would be a tremendous advance in treating locally advanced HNC. This study utilized a sensitive and portable thermal imaging system to establish parameters that will guide development of this technology as a prediction tool in this setting. We explored different approaches and image planes to find that early increases in temperature within an area of interest are associated with more severe mucositis towards the end of therapy. Therefore, thermal imaging could one day be utilized to identify patients at greatest risk for toxicity and its subsequent sequelae of malnutrition, poor pain control, or treatment interruption.

Nonetheless, further studies are warranted before one could universally recommend this technology. The relationship between early change in T and mucositis was statistically significant. However, this association appeared only modest in terms of absolute change. There are likely several reasons underlying this. The mucositis grading system utilized has a small dynamic range (0-4) with the majority of subjects developing grade 3 mucositis at some point on these chemoradiotherapy regimens. More specific grading systems with a wider scoring range should be utilized in future studies as well as patient reported quality of life outcomes. Furthermore, there is no doubt that all the manifestations of mucositis are not reflected by changes in temperature. Although the instrument could detect small changes in temperature, this is still a surrogate for the inflammatory processes underlying mucosal injury.

A peripheral observation of this study is that tumors themselves often displayed higher temperatures than surrounding normal tissue. Thermal imaging technology has been explored for early detection and diagnosis of other cancers, mostly breast and skin malignancies[18,19], but not HNC. Considering the current shortcomings of oral cancer screening[20], another potential application of this thermal imaging device could be in this area. Additionally, early changes in tumor temperature over time may indicate early response allowing for adaptive treatment strategies. These applications would require further development and their implementation presently would not be indicated.

Therefore, this pilot study demonstrated that thermal imaging demands further attention as a tool to predict toxicity in patients treated for locally advanced HNC. Undoubtedly, any predictive tool for development of toxicity would be greatly enhanced by preventative interventions that would mitigate undesired treatment sequelae. The ultimate goal would be

to couple predictive tools such as thermal imaging with interventions that would avoid severe mucositis in patients being treated with chemoradiotherapy.

Supplementary Material

Refer to Web version on PubMed Central for supplementary material.

Acknowledgments

The work at Argonne National Laboratory was supported by UChicago Argonne, LLC, Operator of Argonne National Laboratory ("Argonne"). Argonne, a U.S. Department of Energy Office of Science Laboratory, is operated under Contract No. DE-AC02-06CH11357.

Supported by NIH grants R21 CA125000 and P30 CA14599

References

1. Jemal A, Murray T, Ward E, et al. Cancer statistics, 2005. CA Cancer J Clin. 2005; 55:10–30. [PubMed: 15661684]
2. Nwizu T, Ghi MG, Cohen EE, et al. The role of chemotherapy in locally advanced head and neck squamous cell carcinoma. Semin Radiat Oncol. 2012; 22:198–206. [PubMed: 22687944]
3. Cohen EE, Lingen MW, Vokes EE. The expanding role of systemic therapy in head and neck cancer. J Clin Oncol. 2004; 22:1743–52. [PubMed: 15117998]
4. Haraf DJ, Rosen FR, Stenson K, et al. Induction chemotherapy followed by concomitant TFHX chemoradiotherapy with reduced dose radiation in advanced head and neck cancer. Clin Cancer Res. 2003; 9:5936–43. [PubMed: 14676118]
5. Vokes EE, Stenson K, Rosen FR, et al. Weekly carboplatin and paclitaxel followed by concomitant paclitaxel, fluorouracil, and hydroxyurea chemoradiotherapy: curative and organpreserving therapy for advanced head and neck cancer. J Clin Oncol. 2003; 21:320–6. [PubMed: 12525525]
6. Trotti A, Bellm LA, Epstein JB, et al. Mucositis incidence, severity and associated outcomes in patients with head and neck cancer receiving radiotherapy with or without chemotherapy: a systematic literature review. Radiother Oncol. 2003; 66:253–62. [PubMed: 12742264]
7. List MA, Stracks J. Quality of life and late toxicities in head and neck cancer. Cancer Treat Res. 2003; 114:331–51. [PubMed: 12619549]
8. Cohen, EE.; H, D.; Stenson, K.; Blair, E.; Brockstein, B.; Mauer, A.; Dekker, A.; Williams, R.; Lester, E.; Vokes, EE. Integration of Gefitinib (G), into a Concurrent Chemoradiation (CRT) Regimen Followed by G Adjuvant Therapy in Patients with Locally Advanced Head and Neck Cancer (HNC) - a Phase II Trial. Annual Meeting of the American Society of Clinical Oncology; Orlando, FL. 2005;
9. Correa CR, Cheung VG. Genetic variation in radiation-induced expression phenotypes. Am J Hum Genet. 2004; 75:885–90. [PubMed: 15359380]
10. Andreassen CN, Alsner J, Overgaard J. Does variability in normal tissue reactions after radiotherapy have a genetic basis--where and how to look for it? Radiother Oncol. 2002; 64:131–40. [PubMed: 12242122]
11. Rubin P, Johnston CJ, Williams JP, et al. A perpetual cascade of cytokines postirradiation leads to pulmonary fibrosis. Int J Radiat Oncol Biol Phys. 1995; 33:99–109. [PubMed: 7642437]
12. Barcellos-Hoff MH. How do tissues respond to damage at the cellular level? The role of cytokines in irradiated tissues. Radiat Res. 1998; 150:S109–20. [PubMed: 9806614]
13. Jiang LJ, Ng EY, Yeo AC, et al. A perspective on medical infrared imaging. J Med Eng Technol. 2005; 29:257–67. [PubMed: 16287675]
14. Head JF, Elliott RL. Infrared imaging: making progress in fulfilling its medical promise. IEEE Eng Med Biol Mag. 2002; 21:80–5. [PubMed: 12613215]
15. Renkielska A, Nowakowski A, Kaczmarek M, et al. Static thermography revisited--an adjunct method for determining the depth of the burn injury. Burns. 2005; 31:768–75. [PubMed: 15990239]

16. Gordiyenko EYV, Pearson J, Bader SD, Novosad V. High-sensitivity, and cost-effective system for infrared imaging. Proceedings of SPIE. 2005:103–108.

17. Yefremenko V, Gordiyenko E, Shustakova G, et al. A broadband imaging system for research applications. Rev Sci Instrum. 2009; 80:056104. [PubMed: 19485541]

18. Herman C, Cetingul MP. Quantitative visualization and detection of skin cancer using dynamic thermal imaging. J Vis Exp. 2011

19. Kontos M, Wilson R, Fentiman I. Digital infrared thermal imaging (DITI) of breast lesions: sensitivity and specificity of detection of primary breast cancers. Clin Radiol. 2011; 66:536–9. [PubMed: 21377664]

20. Rethman MP, Carpenter W, Cohen EE, et al. Evidence-based clinical recommendations regarding screening for oral squamous cell carcinomas. Tex Dent J. 2012; 129:491–507. [PubMed: 22779205]

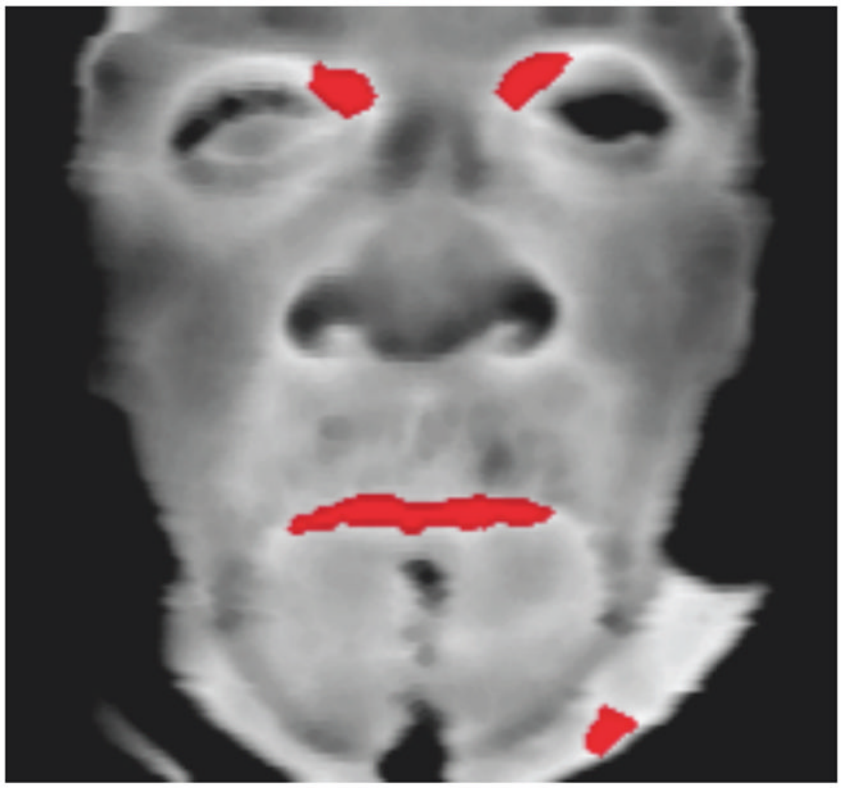

Fig 1.
Frontal thermal image (before CRT). Reference spots (red spots near eyes) have temperature T≥ 0.98 (Tmax) eyes.

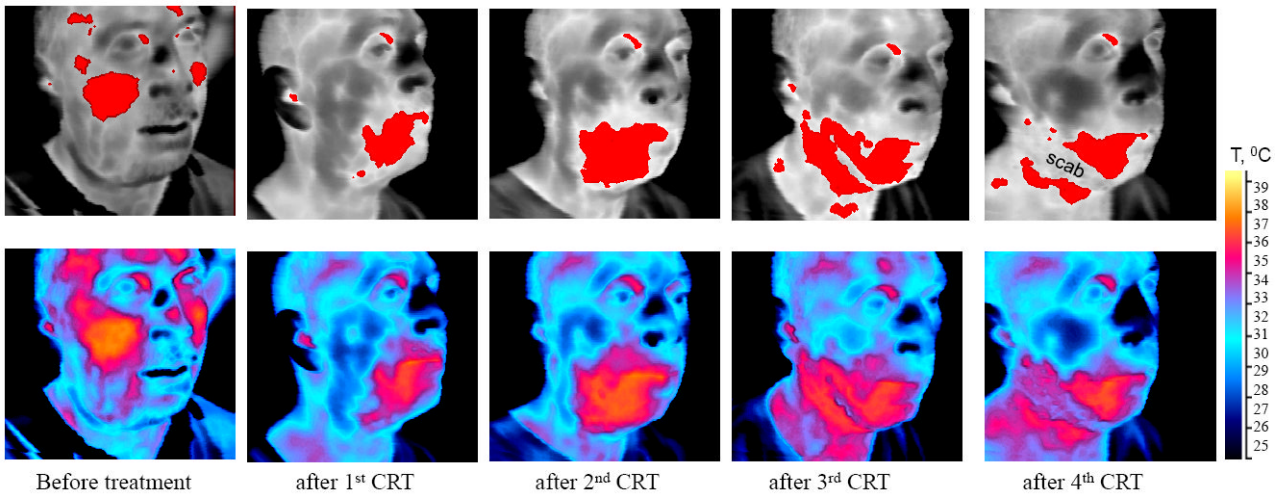

Fig.2.

Red areas on the top series of images correspond to skin temperature T ≥ Tref. Bottom series are scaled in absolute temperature.

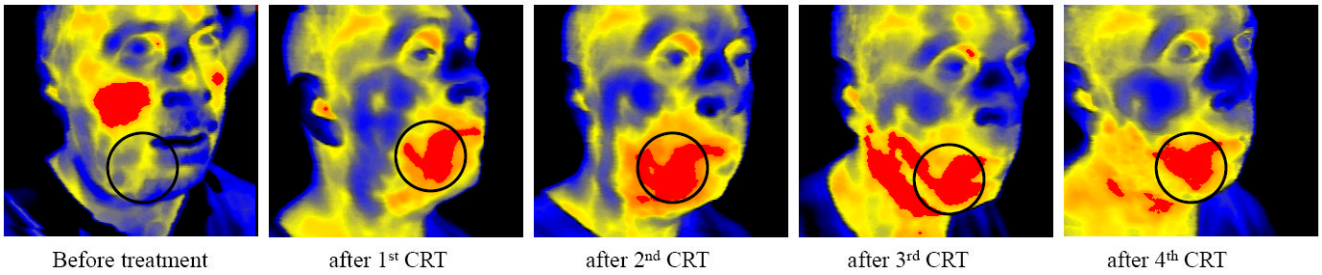

Fig.3.
The series of images with marked “areas of interest” for approach #1 (red regions) and for approach #2 (circled regions)

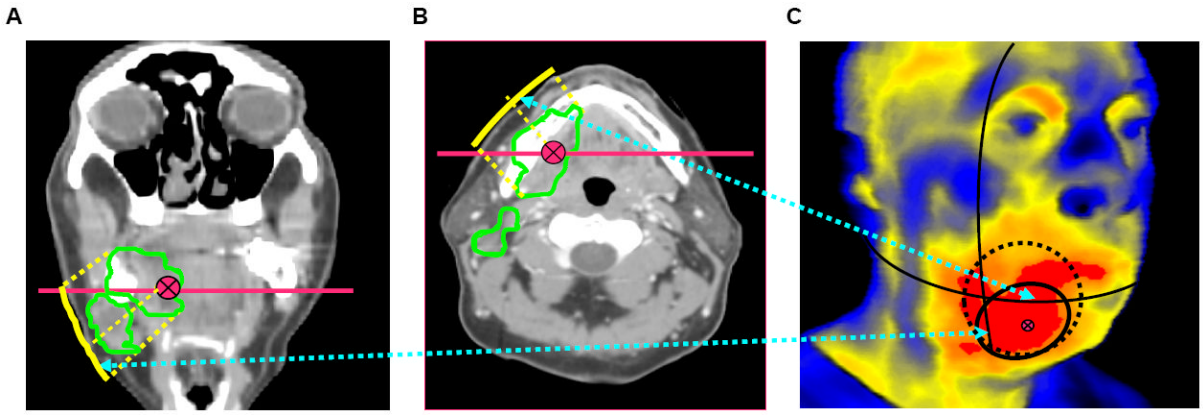

Fig.4. Definition of "area of interest for approach #3"

(A,B) Left and middle pictures represent coronal and transverse sections of patient's head/neck. Red straight lines show cross section locations; green curves outline cross sections of "radiation space of interest"; red point represents"irradiation point of interest"; yellow curve represents geometrical projection on the closest surface. **(C)** On the corresponding thermal image (on the right), solid black circle represents "area of interest for approach #3" approximately calculated from projections. For comparison, on the thermal image are shown "areas of interest" for other approaches: red region – for approach #1, dashed circle – for approach #2.

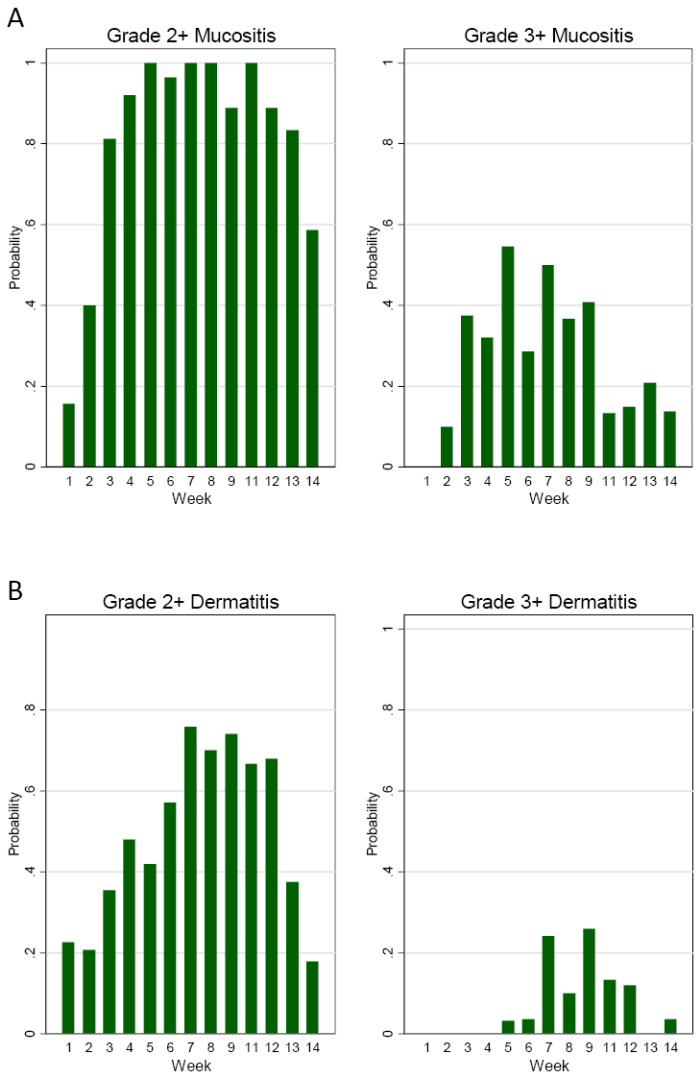

Figure 5.

(A) Proportion of patients with Grade 2+ or Grade 3+ mucositis during treatment (week 1-9) and follow-up (weeks 11-14) using NCI-CTCAE 3.0. **(B)** Proportion of patients with Grade 2+ or Grade 3+ Dermatitis during treatment (weeks 1-9) and follow up (weeks 11-14).

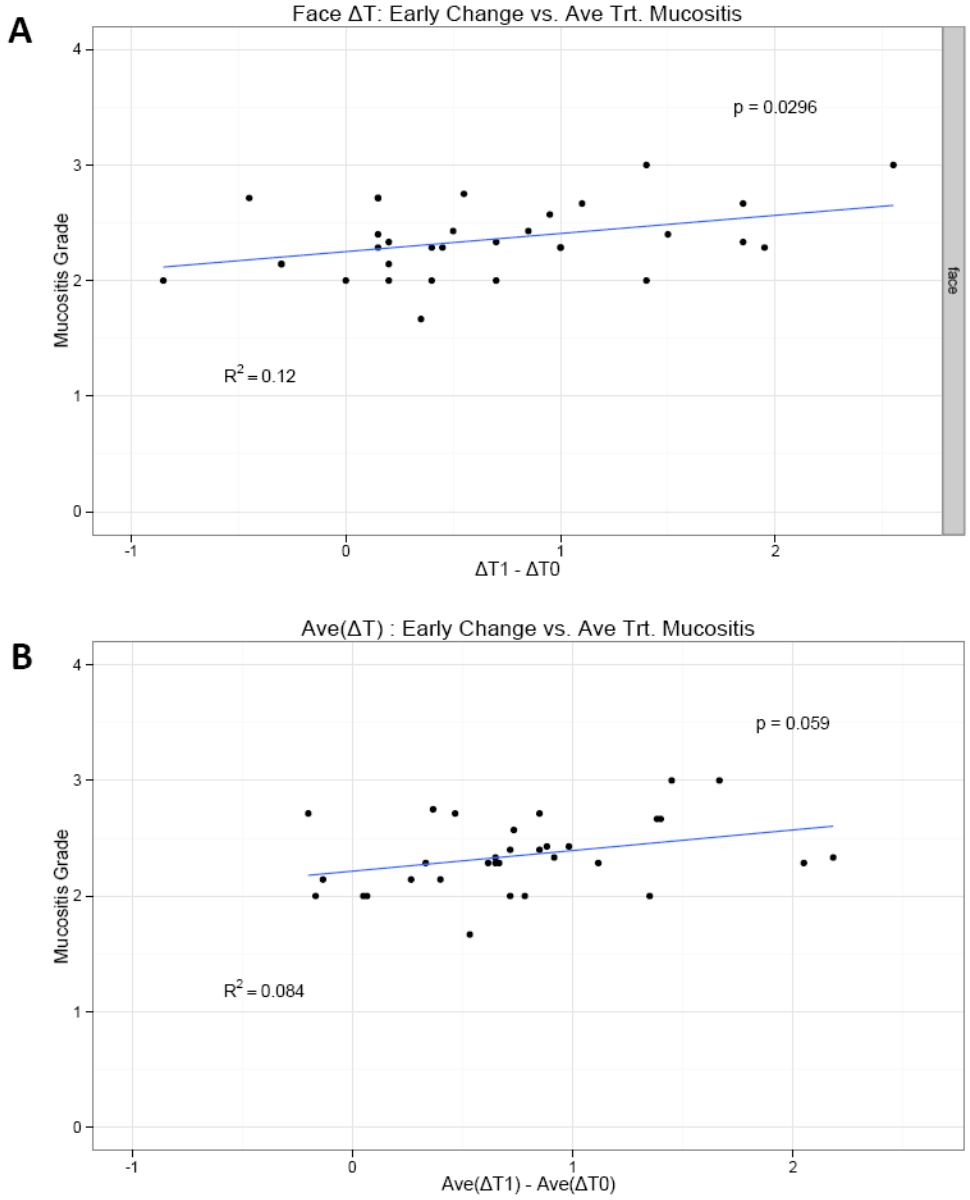

Figure 6.

Based on approach #2- **(A)**- The association between early change in ΔT (i.e. ΔT1-ΔT0, where ΔT1 is the measurement at the end of cycle 1, and ΔT0 is the baseline measurement) and mucositis grade is statistically significant (p=0.03) for Face images, based on separate linear regression models for each image type (p values are reported). On average, for 1 unit increase in (ΔT1-ΔT0), the average mucositis grade during treatment (cycles 2-5) increases by 0.157.

(B)- if we consider early changes in the average temperature (over 3 images) ΔT, i.e. Ave(ΔT1) − Ave (ΔT0), we find a borderline statistically significant correlation with mucositis grade for Approach 2 (pval=0.06). For each unit increase in Ave(ΔT1) − Ave(ΔT0), the average mucositis grade during treatment increases by 0.178.

Table 1

Patient Characteristics

	N	% of Patients
Race		
Caucasian	31	91%
African American	3	9%
Sex		
Male	28	82%
Female	6	18%
Age		
20-40	2	6%
40-60	17	50%
60-80	15	44%
Tx. Regimen		
Cetux FHX	13	38%
DeCIDE	9	26%
off-TFHX	12	35%

*Average Overall Radiation Dose= 74 Gy